Physics Letters B 703 (2011) 34–39

Contents lists available at ScienceDirect

Physics Letters B

www.elsevier.com/locate/physletb

Magnetic and quadrupole moments of neutron deficient $^{58-62}$Cu isotopes

P. Vingerhoets [a], K.T. Flanagan [b,*], J. Billowes [b], M.L. Bissell [a], K. Blaum [c], B. Cheal [b], M. De Rydt [a], D.H. Forest [d], Ch. Geppert [e], M. Honma [f], M. Kowalska [g], J. Krämer [e], K. Kreim [c], A. Krieger [e], R. Neugart [e], G. Neyens [a], W. Nörtershäuser [h,e], J. Papuga [a], T.J. Procter [b], M.M. Rajabali [a], R. Sánchez [h,e], H.H. Stroke [i], D.T. Yordanov [g]

[a] *Instituut voor Kern- en Stralingsfysica, K. U. Leuven, B-3001 Leuven, Belgium*
[b] *School of Physics and Astronomy, University of Manchester, Manchester, M13 9PL, UK*
[c] *Max-Planck-Institut für Kernphysik, D-69117 Heidelberg, Germany*
[d] *School of Physics and Astronomy, University of Birmingham, Birmingham, B15 2TT, UK*
[e] *Institut für Kernchemie, Universität Mainz, D-55128 Mainz, Germany*
[f] *Center for Mathematical Sciences, University of Aizu, Fukushima 965-8580, Japan*
[g] *Physics Department, CERN, CH-1211 Geneva 23, Switzerland*
[h] *GSI Helmholtzzentrum für Schwerionenforschung GmbH, D-64291 Darmstadt, Germany*
[i] *Department of Physics, New York University, New York, NY 10003, USA*

ARTICLE INFO

Article history:
Received 19 April 2011
Received in revised form 18 July 2011
Accepted 20 July 2011
Available online 26 July 2011
Editor: D.F. Geesaman

Keywords:
Hyperfine structure
Nuclear moments
Nuclear spin
Laser spectroscopy
$N = 28$
Shell model

ABSTRACT

This paper reports on the ground state nuclear moments measured in $^{58-62}$Cu using collinear laser spectroscopy at the ISOLDE facility. The quadrupole moments for $^{58-60}$Cu have been measured for the first time as $Q(^{58}\text{Cu}) = -15(3)$ efm^2, $Q(^{59}\text{Cu}) = -19.3(19)$ efm^2, $Q(^{60}\text{Cu}) = +11.6(12)$ efm^2 and with higher precision for ^{61,62}Cu as $Q(^{61}\text{Cu}) = -21.1(10)$ efm^2, $Q(^{62}\text{Cu}) = -2.2(4)$ efm^2. The magnetic moments of ^{58,59}Cu are measured with a higher precision as $\mu(^{58}\text{Cu}) = +0.570(2)\mu_N$ and $\mu(^{59}\text{Cu}) = +1.8910(9)\mu_N$. The experimental nuclear moments are compared to large-scale shell-model calculations with the GXPF1 and GXPF1A effective interactions, allowing the softness of the ^{56}Ni core to be studied.

The advent and continued development of radioactive beam facilities has permitted a revolution in both experimental and theoretical nuclear physics through unprecedented access to rare isotopes [1]. This has allowed compelling questions related to the evolution of nuclear shell structure with neutron or proton excess to be investigated. Regions around doubly magic nuclei present particularly interesting testing grounds due to the relatively small model spaces required to calculate the nuclear observables. The $N, Z = 28$ magic number is the first to arise as a result of the spin-orbit interaction term in the shell model and hence the region around the $N, Z = 28$ doubly magic ^{56}Ni is of considerable interest. Previous experimental and theoretical work has demonstrated that the ^{56}Ni core is relatively soft compared to other doubly magic systems [2–5]. This region has been described as an "active-two-shell" problem rather than one with an inert ^{56}Ni core [6]. Earlier effective interactions used in shell-model calculations applied to the pf-shell such as KB3 [7] and KB3G [8] introduced modifications to the monopole part of the microscopic interaction to successfully describe lighter pf nuclei ($A \leqslant 52$) but still failed close to ^{56}Ni. An alternative method for modifying the microscopic interaction employs an empirical fit to experimental energy levels to produce an effective interaction. The GXPF1 interaction deduced for the full pf-shell [9,10], has proved very successful in describing the properties of isotopes in the pf-shell, including those of yrast states in ^{56,57,58}Ni [9]. A modification to the GXPF1 effective interaction was made, mainly related to the monopole paring interaction, in order to reproduce the excitation energy scheme of ^{56}Ti [11]. The modified interaction, called GXPF1A [12], was aimed at not changing too much the properties of the other isotopes in the pf-shell. Comparison of different nuclear observables in the neutron deficient Cu

* Corresponding author.
E-mail address: kieran.flanagan-2@manchester.ac.uk (K.T. Flanagan).

0370-2693 © 2011 Published by Elsevier B.V. Open access under CC BY license.
doi:10.1016/j.physletb.2011.07.050

isotopes ($Z = 29$) provides a very good test for these interactions and allows to further investigate the role of the monopole term and the influence of correlations.

This Letter reports on new measurements of the magnetic and quadrupole moments of $^{58-62}$Cu isotopes using the high-resolution collinear laser spectroscopy method. A comparison is made between the experimental magnetic and quadrupole moments of the $^{57-69}$Cu ground states (from $N = 28$ to $N = 40$) with the calculated values from large scale shell-model calculations based on the GXPF1 and GXPF1A effective interactions. Magnetic dipole and electric quadrupole moments are sensitive to the detailed composition of the nuclear wave function. Both provide critical tests for the shell-model interaction and model space used. The quadrupole moment has an increased sensitivity to collectivity in the wave function and is therefore a key element when studying the relative softness of the ^{56}Ni core [13].

Collinear laser spectroscopy [14,15] was used to measure the nuclear moments of the neutron deficient Cu isotopes at the ISOLDE facility, CERN. A detailed description of the experimental technique and set-up is presented by Vingerhoets et al. in [16]. The radioactive isotopes were produced through spallation reactions induced by bombarding a ZrO_2 fibre target with 1.4 GeV protons [17]. The RILIS laser ion source was used to resonantly laser ionize the Cu atoms within the hot cavity ionizer (∼2000 °C) [18]. The ions were accelerated through 30 kV and mass separated by the high-resolution separator (HRS) and injected into an RFQ linear gas-filled Paul trap (ISCOOL) [19]. The technique of ion trapping, when applied to collinear laser spectroscopy, can reduce the detected photon background associated with non-resonant scattered laser light. The background reduction factor is defined by the ratio of the bunching time to the bunch width and can reach up to 10^4 [20]. In this work the ions were trapped in ISCOOL for up to 50 ms and released as a bunch with a temporal FWHM of ∼3 μs in the laser interaction region. Typically a ∼ 2 pA beam was injected into ISCOOL to reach these conditions. The ion bunch was neutralized in a sodium vapor cell and overlapped collinearly with the laser beam. A scanning voltage was applied to the charge exchange cell to Doppler tune the ion beam. During the experiment, a gate of 6 μs was placed on the signal from the two photomultiplier tubes. The hyperfine structure of the $^2S_{1/2}$–$^2P_{3/2}$ (324.754 nm) transition in Cu was studied with an external cavity (Spectra-Physics Wavetrain) frequency-doubled continuous wave (CW) dye laser (Coherent 699). The laser was frequency locked to 15409.046 cm^{-1} using an external scanning Fabry–Perot Interferometer (FPI), which was in turn locked to a frequency stabilized HeNe laser. Under such a locking system the drift in the laser is determined by the stability of the HeNe laser, which had a drift of no greater than 3 MHz in an 8 hour period. A wavemeter (Bristol 621) with a specified accuracy of 0.2 parts per million was used to monitor the laser lock.

Analysis of the hyperfine spectra used the description of the energy splitting according to the formulation by Schwartz [21]. The energy splitting of the hyperfine states is summarized by

$$E_F/h = \frac{1}{2}AK + B\frac{\frac{3}{4}K(K+1) - I(I+1)J(J+1)}{2I(2I-1)J(2J-1)} \quad (1)$$

where $K = F(F+1) - I(I+1) - J(J+1)$ and the quantum number F arises from the coupling of I and J where I is the nuclear spin and J is the total electronic angular momentum. The A and B factors are related to the nuclear magnetic dipole and electric quadrupole moment by

$$A = \frac{\mu B_J}{hIJ}, \qquad B = \frac{Q_s V_{zz}}{h}, \quad (2)$$

where μ is the magnetic dipole moment, Q_s is the spectroscopic quadrupole moment, B_J and V_{zz} are the electron-induced magnetic field and the electric field gradient at the nucleus, respectively. The spectra were fitted to Eq. (1) using the MINUIT routine [22] and an example for ^{59}Cu is shown in Fig. 1. A summary of the measured A and B values is given in Table 1. The estimated systematic error of 10^{-4} is dominated by the uncertainty in measuring the total accelerating voltage, which includes the uncertainty in the voltage applied to the neutralization cell and ion trap region in ISCOOL. This error is smaller than the recorded statistical error. Considering that the best precision of these measurements is of the order of 5×10^{-4}, the small hyperfine anomaly (e.g. $^{63}\Delta^{65} = 4.7(2) \times 10^{-5}$ [23] and $^{59}\Delta^{69} = 12(17) \times 10^{-4}$ [24]) has been ignored. This allows the nuclear magnetic dipole and electric quadrupole moments to be extracted from the A and B factors by using the ratio with the literature values for stable ^{65}Cu: $A_{\text{ref}} = +6284.405(5)$ MHz, $B_{\text{ref}} = -25.9(4)$ MHz, $\mu_{\text{ref}} = +2.3817(3)\mu_N$ and $Q_{\text{ref}} = -19.5(4)$ efm^2 [25–27]. The nuclear moments deduced from this analysis are summarized in Table 2 and compared to literature values where they exist. The magnetic dipole moments for ^{58,59}Cu deviate significantly from those previously measured using in-gas-cell laser spectroscopy [28].

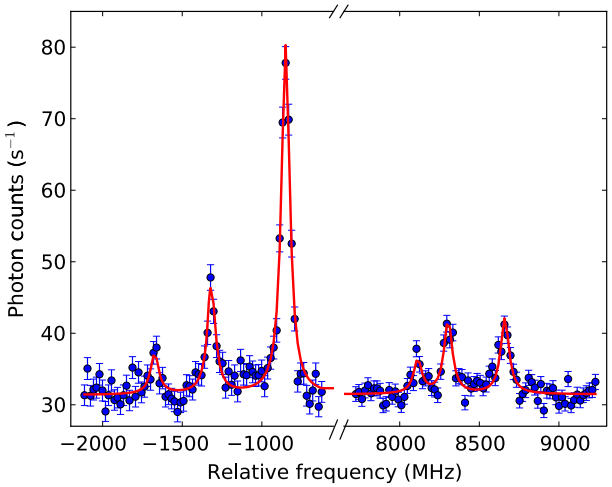

Fig. 1. (Color online.) Hyperfine spectrum of the $^2S_{1/2}$–$^2P_{3/2}$ (324.754 nm) in ^{59}Cu showing the fit as a solid line. The fit to the data minimized χ^2 with 147 degrees of freedom, which resulted in a (normalized) $\chi^2 = 1.4$.

Table 1
Summary of the measured ground-state hyperfine parameters of the $^2S_{1/2}$–$^2P_{3/2}$ transition in Cu.

Isotope	I^π	$A(^2S_{1/2})$ (MHz)	$A(^2P_{3/2})$ (MHz)	$B(^2P_{3/2})$ (MHz)
^{58}Cu	1^+	+2257(9)	+77(3)	−20(4)
^{59}Cu	$3/2^-$	+4989.6(24)	+164.6(9)	−25.7(24)
^{60}Cu	2^+	+2411.6(10)	+78.8(3)	+15.4(16)
^{61}Cu	$3/2^-$	+5562.9(14)	+183.8(4)	−28.0(10)
^{62}Cu	1^+	−1502.4(14)	−48.2(5)	−2.9(5)

The difference between magnetic moments reported here and in literature is highlighted for ^{58}Cu in Fig. 2, where the dotted line represents the hyperfine splitting for this transition simulated with the magnetic moment reported by Cocolios et al. [28], which is also consistent with the result of Mihara et al. using β-NMR [29]. In addition, the inset plot in Fig. 2 shows the data collected in that region from 3700 to 4200 MHz. These data were collected for approximately the same time as the main plot, but with a bunching time of 200 ms instead of 50 ms, and hence the improved background suppression. With these data it is possible to exclude hyperfine resonances in this region. Note that the resolution in the

Table 2
Summary of the measured ground-state nuclear moments. The previous values quoted from Ref. [16] represent preliminary measurements and have not been used to further improve the precision of the new measurements reported here.

Isotope	I^π	$\mu_{\rm exp}(\mu_N)$	$\mu_{\rm lit}(\mu_N)$	Ref.	$Q_{\rm exp}$ (efm^2)	$Q_{\rm lit}$ (efm^2)	Ref.
^{58}Cu	1^+	+0.570(2)	+0.479(13)	[28]	−15(3)		
			+0.46(3)	[29]			
			+0.52(8)	[30]			
^{59}Cu	$3/2^-$	+1.8910(9)	+1.910(4)	[28]	−19.3(19)		
			+1.84(3)	[30]			
			+1.891(9)	[31]			
^{60}Cu	2^+	+1.2186(5)	+1.219(3)	[25]	+11.6(12)		
^{61}Cu	$3/2^-$	+2.1083(5)	+2.1089(11)	[16]	−21.1(10)	−21(2)	[16]
			+2.14(4)	[25]			
^{62}Cu	1^+	−0.3796(4)	−0.3809(12)	[16]	−2.2(4)	0(2)	[16]
			−0.380(4)	[25]			

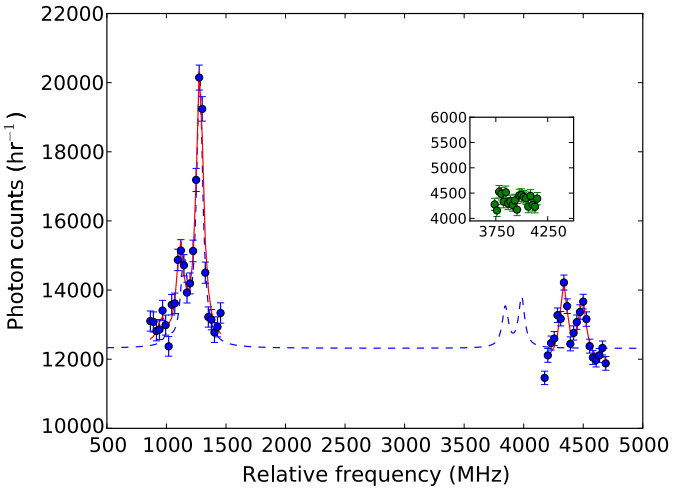

Fig. 2. (Color online.) Hyperfine spectrum of $^2S_{1/2}$–$^2P_{3/2}$ transition in ^{58}Cu showing the fit (with transition intensities as free parameters) as a solid line. The dashed line corresponds to a simulated hyperfine spectrum using the magnetic moment reported by Cocolios et al. [28]. The intensity of the simulated spectrum has been fixed to match the most intense peak ($F = 3/2 \rightarrow F = 5/2$) in the measured spectrum, all other peaks use angular momentum coupling considerations relative to this transition. The insert shows the data collected in the range 3750–4200 MHz, excluding a hyperfine resonance in this region.

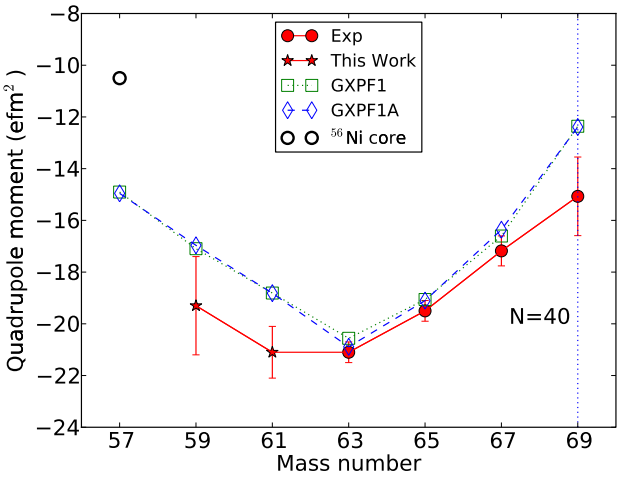

Fig. 3. (Color online.) The odd–even quadrupole moments reveal that the ^{56}Ni core is even softer than predicted by the theoretical calculations. The open circle for ^{57}Cu corresponds to the single-particle quadrupole moment calculated with a ^{56}Ni core. The effective charges used in these calculations were $e_p = 1.5e$, $e_n = 0.5e$. Experimental values for ^{67,69}Cu were taken from [16].

collinear method is better than 100 MHz, whereas it is only 2 GHz with the gas-cell technique.

The moments of the more neutron-rich ^{61}Cu–^{75}Cu isotopes were previously compared to large scale shell model calculations using the jj44b [32] and JUN45 [33] effective interactions, which operate in the $f_{5/2}$, $p_{1/2,3/2}$, $g_{9/2}$ ($f5pg9$) model space, starting from an inert ^{56}Ni core [16,34,35]. Both calculations successfully describe the migration of the $\pi f_{5/2}$ state as the $\nu g_{9/2}$ orbital is filled [34] and give a reasonable agreement for the nuclear magnetic and quadrupole moments in the Cu and Ga isotopes over the full neutron range [34–37]. However, because $N, Z = 28$ is considered to be a closed shell in these calculations, the agreement deteriorates significantly towards ^{57}Cu [16]. Recently a new effective interaction has been published for this mass region, starting from a ^{48}Ca core (still excluding neutron excitations across $N = 28$, but including proton excitations across $Z = 28$) [38]. It would be interesting to compare the previous and new data to these calculations to provide further information on the $N = 28$ shell gap.

In this Letter, the experimental results are compared to shell-model calculations using the GXPF1 [6,9] effective interaction and its modification GXPF1A [12]. The GXPF1 effective interaction considers the full pf shell as a model space, with ^{40}Ca as a core. The GXPF1 interaction can be specified uniquely in terms of four single-particle energies of the $f_{7/2}$, $p_{3/2}$, $f_{5/2}$ and $p_{1/2}$ orbits and

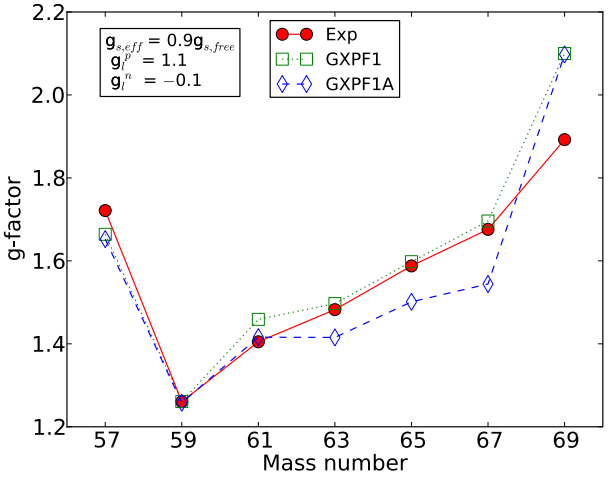

Fig. 4. (Color online.) The experimental odd–even g-factors (solid circles) are compared with calculations for the GXPF1 (open squares) and GXPF1A (open diamonds) interactions. The experimental data point at ^{57}Cu is taken from [40] and the data for ^{67,69}Cu were taken from [16].

195 two-body matrix elements (TBME) [9]. Starting values for the TBME were taken from the realistic G-matrix interaction based on the Bonn-C potential [39]. Selected 70 linear combinations of the single-particle energies (SPE) and TBME were fitted to 699 binding

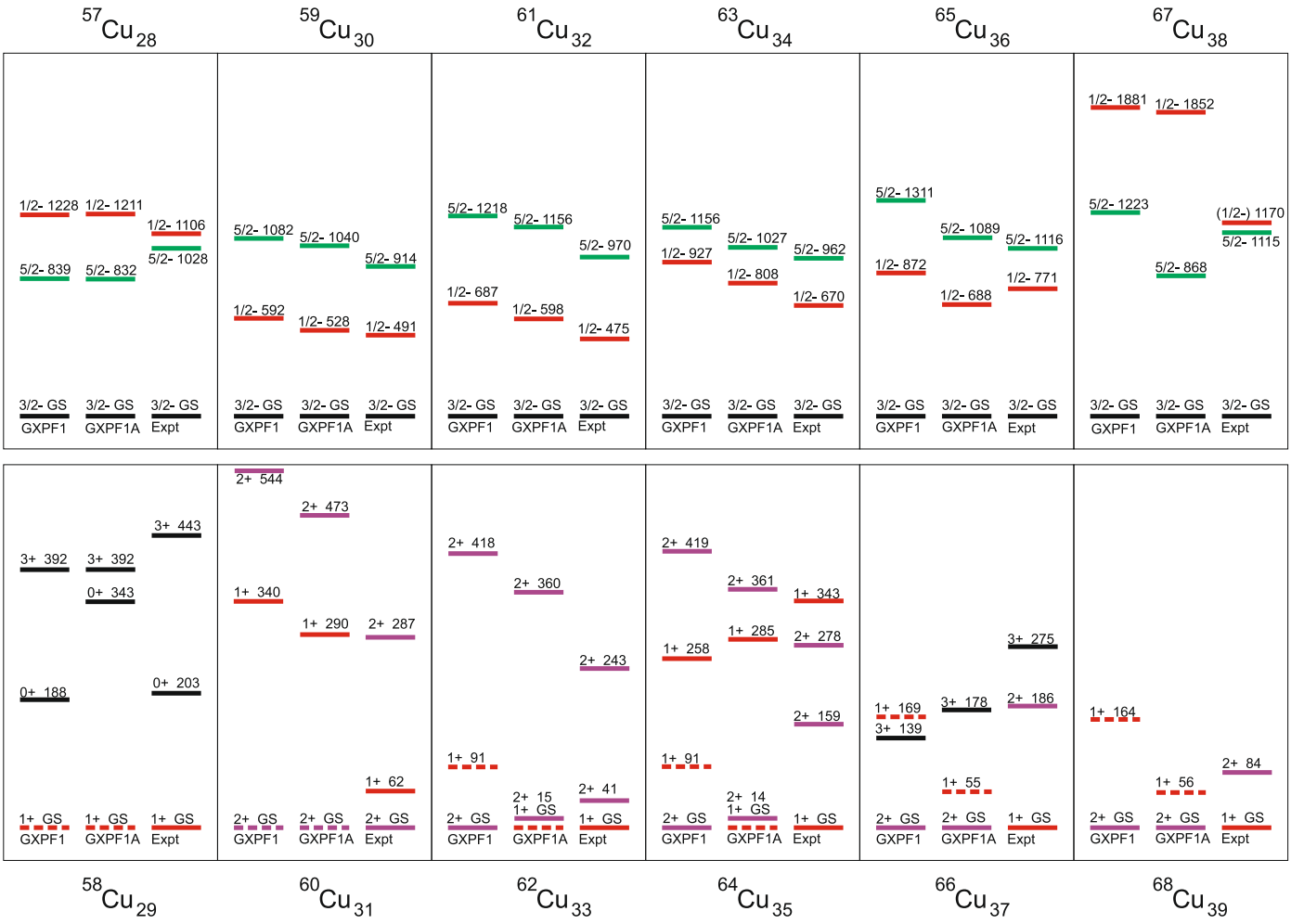

Fig. 5. (Color online.) The experimental and calculated low-lying energy levels (in keV) for the neutron-deficient odd–even and odd–odd Cu isotopes [41]. The ground state of the odd–odd isotopes is not always correctly identified by either the GXPF1A or GXPF1 interactions. The states used in the g-factor plot are indicated with a dashed line.

and excitation energies in the region, from ^{47}Ca up to ^{65}Ge, including $^{58-63}$Cu. The fitting procedure is outlined in [10]. The GXPF1 interaction was tested extensively and proved to be very successful in the description of a variety of parameters such as binding energies, magnetic moments, quadrupole moments, 2^+ excitation energies and transition strengths [6]. Some discrepancy in the binding energies for nuclei with $Z \geqslant 32$ and $N \geqslant 35$ indicated its limitations towards the end of the pf shell. An increase in the $E(2+)$ excitation energies for Ca, Ti and Cr isotopes at $N = 32$ was correctly predicted by the GXPF1 interaction. However, for Ca and Ti, GXPF1 predicts another increase at $N = 34$. This was found to be in discrepancy with experiment for the case of ^{56}Ti [11] and therefore, a modification to the GXPF1 interaction was presented [12]. Modifications in the $T = 1$ two-body matrix elements were made, mainly related to the monopole pairing interaction. The pair scattering among the $p_{1/2}$ and the $f_{5/2}$ orbits has been reduced. Furthermore, the effective single-particle energy (ESPE) of the $\pi p_{1/2}$ orbit is modified for isotopes with $N > 32$, leading to a reduction of the gap between the $p_{1/2}$ and the $f_{5/2}$ orbits at $N = 34$ by 0.5 MeV [12]. Finally, in the GXPF1A interaction the strength of the quadrupole–quadrupole interaction between the $p_{1/2}$ and $f_{5/2}$ is increased. This was done in analogy with several nuclei outside a ^{56}Ni core, where an enhanced quadrupole–quadrupole interaction compared to the original G-matrix interaction led to a successful description of 2^+ states [6]. Note that for both interactions the ESPE of the $\pi 2p_{1/2}$ orbit is lower than that of the $\pi 1f_{5/2}$ orbit for the elements Ca, Ti, and Cr over the full neutron range. In the Cu isotope chain however, this order is reversed in the isotopes below $N = 32$, but the $p_{1/2}$ remains below $f_{5/2}$ in the isotopes around $N = 32$–34. The reduction of this energy gap in the ESPE will have a significant influence on the composition of the Cu wave functions, as will be illustrated further.

In Fig. 3 the quadrupole moments are compared with predictions by the GXPF1 and GXPF1A interactions. The standard effective charges as adopted in [6] have been used. The calculated quadrupole moment of ^{57}Cu, assuming a rigid ^{56}Ni core (open circle in Fig. 3) is significantly smaller than the values based on a ^{40}Ca core, illustrating the effect of core excitations on the quadrupole moments of odd–even Cu isotopes. Even including such excitations, the calculated core polarization for ^{59,61}Cu is still less than experimentally observed, suggesting that excitations across $N, Z = 28$ are even more important than presently assumed with GXPF1.

Although several TBME were changed between the GXPF1 and GXPF1A interactions, the predicted quadrupole moments are very similar. This is because changes in proton and neutron contribution to the quadrupole moment cancel each other. The proton quadrupole moment is dominated by the negative single-particle quadrupole moment of the $p_{3/2}$ orbit. As this single-particle component is reduced in the wave functions calculated with the GXPF1A interaction, the proton quadrupole moment is decreased. However, in GXPF1A the pairing interaction for the $p_{1/2}$–$p_{1/2}$ and

the $p_{1/2}$–$f_{5/2}$ neutron orbits is made less attractive, relatively suppressing formation of 0^+ pairs in these orbits. In addition, the quadrupole–quadrupole interaction for these orbits is made more attractive [12], which should promote the formation of broken-pair particle-hole components in the wave function. Such collective quadrupole correlation can enhance the neutron collectivity and thus the neutron component of the quadrupole moment.

The g-factors of the odd–even Cu isotopes are given in Fig. 4. The agreement with experiment is very good for the GXPF1 interaction. The discrepancy at ^{69}Cu is due to excitations across $N = 40$ which are not included in the model space. The GXPF1A interaction however, underestimates the g-factor trend at $^{63-67}$Cu. That is because the collectivity of the neutron $\nu p_{1/2}$ and $\nu f_{5/2}$ orbits is enhanced for GXPF1A. This reduces the positive neutron single-particle contribution from $N = 34$ onwards, which brings these magnetic moments closer to the (smaller) values of the 2^+ state in the even–even Ni core. This is seen in Fig. 4, where the g-factor is less positive than the GXPF1 value from ^{63}Cu onwards, where the $\nu p_{1/2}$ and $\nu f_{5/2}$ orbits start to get filled.

In Fig. 5 the energy levels for the odd–even isotopes are shown. The energy levels predicted by the GXPF1A interaction are consistently lower than the GXPF1 levels. This is in line with the reduction of the pairing strength within the $f_{7/2}$ orbit for the GXPF1A interaction. Pair scattering into the $p_{3/2}$ orbit is enhanced, making it more favorable for the single proton to excite to the $f_{5/2}$ or the $p_{1/2}$ orbit than with an inert ^{56}Ni core. The combination of the g-factor trend with the energy levels for the odd–even isotopes clearly indicates that a change in TBME can be made to achieve better description of experimental data, but the agreement with experiment is not necessarily true for every parameter. In this case, the excitation energies of the $5/2^-$ and the $1/2^-$ states are better described by the GXPF1A interaction, however the g-factor trend clearly shows that there is still a structural problem with the modification of the TBME. This illustrates the sensitivity of the magnetic moments to the detailed composition of the wave function.

The g-factors of the odd–odd Cu isotopes are given in Fig. 6. All values are very well reproduced by the GXPF1 interaction, except for ^{64}Cu which deviates a little. That is due to a configuration mixing with another low-lying 1^+ state that is not fully accounted for in the calculation. For the GXPF1A interaction, this mixing is also not correctly taken into account for ^{66}Cu.

The odd–odd isotopes levels and their excitation energies are shown in Fig. 5. The calculated ordering of states with either the GXPF1 or GXPF1A interactions, does not always correctly identify the ground state. The state which is used in the g-factor plot is indicated with a dashed line. As in the case of the odd–even Cu isotopes, it can be seen that the GXPF1A reproduces better the experimental energy levels, but the g-factor trend reveals that the composition of the wave function of the ground state is not correct. The combination of magnetic moments and energy levels again provides different viewpoints to evaluate large-scale shell-model calculations.

Finally, the odd–odd neutron-deficient quadrupole moments are given in Fig. 7. Again the GXPF1 interaction reproduces most values extremely well, but for ^{64,66}Cu there is some discrepancy. The modifications made in the GXPF1A interaction do not strongly affect the ^{58,60,68}Cu quadrupole moments, but lead to a better agreement with experiment for ^{66}Cu and worse agreement for ^{64}Cu. In the case of ^{64}Cu this also leads to a reversal in the sign of the quadrupole moment.

In conclusion, collinear laser spectroscopy with bunched atomic beams has been used to study the neutron deficient Cu isotopes. This work has measured the quadrupole moments down to ^{58}Cu and higher precision measurements in ^{61,62}Cu. The high resolution

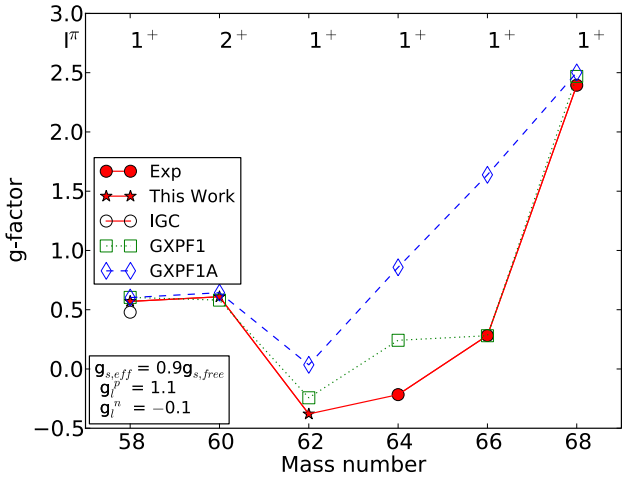

Fig. 6. (Color online.) The g-factors for the neutron-deficient odd–odd Cu isotopes. The difference between GXPF1A calculations and the experimental g-factors for ^{64,66}Cu arises due to mixing between the ground state and a low-lying 1^+ state, which is not fully accounted for by theory. The experimental data points for ^{64,66,68}Cu were taken from [16]. The value measured using the in-gas cell laser spectroscopy technique (IGC) was taken from Cocolios et al. [28].

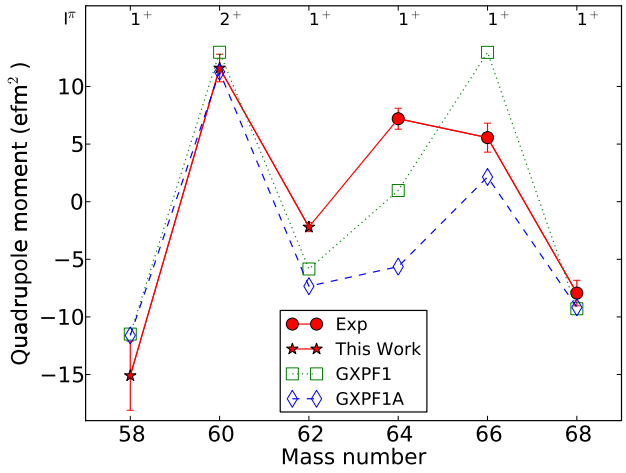

Fig. 7. (Color online.) The odd–odd Cu quadrupole moments compared with theory. The deviation for the GXPF1A interaction is due to mixing of 1^+ states, which is not fully accounted for by theory. The effective charges used in these calculations were $e_p = 1.5e$, $e_n = 0.5e$. The experimental data points for ^{64,66,68}Cu were taken from [16].

afforded by the collinear technique has permitted the magnetic moments of ^{58,59}Cu to be remeasured with higher precision ($>\sim 4$ times) and accuracy, demonstrating a considerable deviation from previous in-source and β-NMR measurements.

The measured moments have been compared to the shell-model results with GXPF1 and GXPF1A effective interactions. The deviation of the experimental quadrupole moments from the shell-model predictions is an indicator of increased core polarization and evidence that the ^{56}Ni core is even softer than previously thought. Ideally a precise measurement of the quadrupole moment of ^{57}Cu would help resolve questions related to the ^{56}Ni core and associated core polarization effects. The measured moments illustrate that the improved description of the energy levels with the GXPF1A interaction does not necessarily lead to better shell-model wave functions in comparison to those with the original GXPF1 interaction. Further theoretical investigation is needed for a comprehensive description.

Acknowledgements

This work has been supported by the German Ministry for Education and Research (BMBF) under Contract No. 06MZ9178I, the UK Science and Technology Facilities Council (STFC), the FWO-Vlaanderen (Belgium), EU Sixth Framework through No. Eurons-506065, BriX IAP Research Program No. P6/23 (Belgium), the Helmholtz Association of German Research Centres (VH-NG-037 and VH-NG-148), the Max-Planck Society and NSF grant PHY-0758099. A. Krieger acknowledges support from the Carl Zeiss Stiftung (AZ:21-0563-2.8/197/1). H.H Stroke acknowledges the donation from E. Schneiderman to New York University. We would like to thank the ISOLDE technical group for their support and assistance during this project.

References

[1] P.V. Duppen, K. Riisager, J. Phys. G 38 (2011) 024005.
[2] J.S. Berryman, et al., Phys. Rev. C 79 (2009) 064305.
[3] A.F. Lisetskiy, et al., Phys. Rev. C 68 (2003) 034316.
[4] T. Otsuka, M. Honma, T. Mizusaki, Phys. Rev. Lett. 81 (1998) 1588.
[5] K.H. Speidel, O. Kenn, F. Nowacki, Prog. Part. Nucl. Phys. B 49 (2002) 91.
[6] M. Honma, T. Otsuka, B.A. Brown, T. Mizusaki, Phys. Rev. C 69 (2004) 034335.
[7] A. Poves, A. Zuker, Phys. Rep. 70 (1981) 235.
[8] A. Poves, J. Sanchez-Solano, E. Caurier, F. Nowacki, Nucl. Phys. A 694 (2001) 157.
[9] M. Honma, T. Otsuka, B.A. Brown, T. Mizusaki, Phys. Rev. C 65 (2002) 061301.
[10] M. Honma, B.A. Brown, T. Mizusaki, T. Otsuka, Nucl. Phys. A 704 (2002) 134.
[11] S.N. Liddick, et al., Phys. Rev. Lett. 92 (2004) 072502.
[12] M. Honma, T. Otsuka, B. Brown, T. Mizusaki, Eur. Phys. J. A 25 (2005) 499.
[13] G. Neyens, Rep. Prog. Phys. 66 (2003) 633.
[14] B. Cheal, K.T. Flanagan, J. Phys. G 37 (2010) 113101.
[15] A.C. Mueller, et al., Nucl. Phys. A 403 (1983) 234.
[16] P. Vingerhoets, et al., Phys. Rev. C 82 (2010) 064311.
[17] U. Köster, et al., Nucl. Instrum. Methods B 204 (2003) 303.
[18] B.A. Marsh, et al., Hyperfine Interact. 196 (2010) 129.
[19] E. Mané, et al., Euro. Phys. J. A 42 (2009) 503.
[20] P. Campbell, et al., Euro. Phys. J. A 15 (2002) 45.
[21] C. Schwartz, Phys. Rev. 97 (1955) 380.
[22] F. James, M. Roos, Comput. Phys. Commun. 10 (1975) 343.
[23] P.R. Locher, Phys. Rev. B 10 (1974) 801.
[24] V.V. Golovko, et al., Phys. Rev. C (2011), doi:10.1103/PhysRevC.84.014323.
[25] P. Raghavan, At. Data Nucl. Data Tables 42 (1989) 189.
[26] J. Ney, Z. Phys. A 196 (1966) 53.
[27] Y. Ting, H. Lew, Phys. Rev. 105 (1957) 581.
[28] T.E. Cocolios, et al., Phys. Rev. C 81 (2010) 014314.
[29] M. Mihara, et al., Hyperfine Interact. 197 (2010) 143.
[30] N.J. Stone, et al., Phys. Rev. C 77 (2008) 067302.
[31] V. Golovko, et al., Phys. Rev. C 70 (2004) 014312.
[32] B.A. Brown, A.F. Lisetskiy, private communication, 2009.
[33] M. Honma, T. Otsuka, T. Mizusaki, M. Hjorth-Jensen, Phys. Rev. C 80 (2009) 064323.
[34] K.T. Flanagan, et al., Phys. Rev. Lett. 103 (2009) 142501.
[35] K.T. Flanagan, et al., Phys. Rev. C 82 (2010) 041302.
[36] B. Cheal, et al., Phys. Rev. Lett. 104 (2010) 252502.
[37] B. Cheal, et al., Phys. Rev. C 82 (2010) 051302.
[38] K. Sieja, F. Nowacki, Phys. Rev. C 81 (2010) 061303.
[39] M. Hjorth-Jensen, T.T.S. Kuo, E. Osnes, Phys. Rep. 261 (1995) 125.
[40] T.E. Cocolios, et al., Phys. Rev. Lett. 103 (2009) 102501.
[41] National Nuclear Data Center, URL http://www.nndc.bnl.gov/.